AxonPacking: an algorithm to simulate realistic arrangement of white matter axons

Tom Mingasson[a,b], Tanguy Duval[a], Nikola Stikov[a,d], Julien Cohen-Adad[a,c]

[a] NeuroPoly Lab. Institute of Biomedical Engineering, Polytechnique Montreal, Montreal, QC, Canada

[b] Ecole Centrale de Nantes, Nantes, France

[c] Functional Neuroimaging Unit, CRIUGM, Université de Montréal, Montreal, QC, Canada

[d] Montreal Heart Institute, Montreal, QC, Canada

Corresponding author : Julien Cohen-Adad. jcohen@polymtl.ca

ABSTRACT

Quantitative MRI can provide parameters that describe white matter microstructure, such as the fiber volume fraction (FVF), the myelin volume fraction (MVF) or the axon volume fraction (AVF) via the fraction of restricted water (*fr*). While already being used for clinical application, the complex interplay between these parameters requires thorough validation via simulations. These simulations required a realistic, controlled and adaptable model of the white matter axons with the surrounding myelin sheath. While there already exist useful algorithms to perform this task, none of them combine optimisation of axon packing, presence of myelin sheath and availability as free and open source software. Here, we introduce a novel disk packing algorithm that addresses these issues.

The performance of the algorithm is tested in term of reproducibility over 50 runs, resulting density, and stability over iterations. This tool was then used to derive multiple values of FVF and to study the impact of this parameter on *fr* and MVF in light of the known microstructure based on histology sample. The standard deviation of the axon density over runs was lower than 10^{-3} and the expected hexagonal packing for monodisperse disks was obtained with a density close to the optimal density (obtained: 0.892, theoretical: 0.907). Using an FVF ranging within [0.58, 0.82] and a mean inter-axon gap ranging within [0.1, 1.1] µm, MVF ranged within [0.32, 0.44] and *fr* ranged within [0.39, 0.71], which is consistent with the histology.

The proposed algorithm is implemented in the open-source software AxonPacking (https://github.com/neuropoly/axonpacking) and can be useful for the study of qMRI methods applied to the peripheral and central nervous system.

Keywords: quantitative MRI; myelin volume; fraction restricted; axon density; disks packing; white matter; microstructure

Highlights:

- AxonPacking: open-source software for simulating white matter microstructure
- Validation on a theoretical disk packing problem.
- Reproducible and stable for various densities and diameter distributions
- Can be used to study interplay between myelin/fiber density and restricted fraction

1. INTRODUCTION

The white matter contains bundles of myelinated nerve cell projections (axons). Over the past years, Magnetic Resonance Imaging (MRI) has seen the development of quantitative metrics that can provide microstructural information about these axons, such as the myelin volume fraction (MVF), the intra-axonal volume fraction via the fraction of restricted water (*fr*), and the ratio of the inner to the outer diameter of the neuronal fibers (g-ratio) in white matter (1–3). However, the realistic ranges for these parameters, as well as their sensitivity to microstructural variation (e.g. changes in axon density, axon diameter distribution, g-ratio) are not clear. While some relationships can be derived using analytical equation (e.g., myelin content can be related to FVF assuming myelin thickness is fixed), other relationships, such as the axon density as a function of the gap between two axons, requires simulations due to the random nature of the problem.

Assuming parallel fibers, which is typical for model-based quantitative diffusion metrics (2), the geometrical simulation of a fiber bundle can be reduced to a two-dimensional polydisperse disks packing problem. Despite the presence of neurite orientation dispersion (4), the 2D reduction can be useful and is already a close representation of what is observed in histology in the case of quasi-parallel fibers (5). Particle packing has been extensively studied in the past decades with a wide spectrum of applications in the fields of physics, industry and mathematics. Examples of applications are the modeling of granular media (6,7) or powder and fluid (8–10) , optimal arrangement of cylindrical products in a container (11) or electrical wires in a bundle (12) or lastly conformal mapping on a surface (13).

While particle packing is a very complex optimization problem (14), multiple approaches exist. Several algorithms were developed in an attempt to simulate packing of identical spheres (15–17) or disks (18,19). In the case of polydisperse disks simulations, a first approach consists of representing a fixed graph of disk centers positions and then finding the configurations of each individual disk diameter satisfying preassigned patterns of tangency (13). However, this approach cannot build packing from a set of particles whose sizes are user-defined. Another approach aims at maximizing the packing of disks of known radius in a rectangle (20,21), a circular region (22) or an arbitrary polygon (23). However, some of these algorithms were developed with specific constraints in mind that are not suitable for the white matter, such as (i) some algorithms place each element (disk or

sphere) within a container which limits the maximal disk density (22) (ii) heuristics methods involve reordering of disks from the largest to the smallest and placing same-sized disks close together in the packing, which does not represent the reality of white matter axons (20,21) (iii) other algorithms modify the initial diameter distribution by adding disks of appropriate size in empty spaces (24). Moreover, many of the proposed algorithms are nonlinear and designed for small sets of disks (under 100) without being easily scalable to larger dimensions (20,21). Algorithms that are relieved from the above-mentioned constraints can be found in the field of particle dynamics (in solid, fluid or gas). Two main methods exist for such simulation: dynamic approaches (molecular dynamic) where the disks are hard or soft particles obeying mechanical and energetic conservation laws (25) and non deterministic approaches based on Boltzmann probabilities (26). In molecular dynamics (MD) particles can be displaced whether synchronously in small time steps and detoured when overlap occurs (time-driven MD) (25), or according to a list of events such as collisions between particles ordered in time (event-driven MD) (27). The event-driven method presents the drawback of requiring to calculate the happening time of a certain collision event for each particle and thus is particularly computationally demanding.

Several simulators were developed for simulating white matter axons. In order to reach high density, Hall and Alexander (28) used iterative diameter increase, which precludes the user from setting a desired axon diameter distribution. Also, the maximal density depends on the initial graph of disks position. Another simulator of water molecule diffusion from Dougherty et al.[1] uses a triangle mesh to determine the position of the axons and thus does not optimize the fiber density. It should be noted that interesting recent work (29) also tries to implement alternative methods to simulate white matter microstructure, but the algorithm is not yet publicly available.

In this paper, we present AxonPacking[2], a novel, easy-to-use and open-source Matlab algorithm for simulating random disk packing with user-defined diameter distribution of axons. This algorithm is based on molecular dynamics without any border constraints. Axon density is optimized by migrating axons towards the center of the 2D space. A couple of inputs and outputs were specifically added to model the white matter realistically: gap between axons, myelin thickness relationship with axon diameter, extraction of myelin volume fraction (MVF), fiber volume fraction (FVF) (i.e. disk density) and fraction of restricted

[1] https://github.com/rfdougherty/dSim
[2] https://github.com/neuropoly/axonpacking

water (*fr*). This simulator was used to extract realistic ranges of MVF and *fr* as compared against histology.

2. METHODS

2.1. White matter model

White matter tissue is divided in three compartments: axons, myelin sheath and extra-axonal space. Axons are assumed to be parallel cylinders, therefore the invariance along the fiber axis makes it possible to consider this problem in 2D. The assumption of parallel fibers is adapted for regions presenting a good coherence of orientation of the neuronal bundles such as in the spinal cord. The dense packing of axons is thus equivalent to the generation of random 2-dimensional packing of N perfectly round and non-compressible disks. As shown in previous histological studies (30,31), axon diameter distributions follow a Gamma distribution (defined by its mean μ and variance σ^2). The Gamma probability for a diameter d is defined as follows (with Γ the Gamma function of Euler): $Prob_{Gamma}(d, \mu, \sigma) = d^{a-1} * exp(-\frac{d}{b}) / (\Gamma(a) * b^a)$ *where* $a = (\mu / \sigma)^2$ *and* $b = \sigma^2 / \mu$.

Axons are spaced from each other by a gap Δ (see definition in figure 1). This gap is assumed constant in our model. Axons are surrounded by a myelin sheath. The ratio of the inner ($d_{unmyelinated}$) to the outer diameter ($d_{myelinated}$) of this myelin sheath is called the fiber g-ratio: $g_{ratio} = d_{unmyelinated} / d_{myelinated}$. Interestingly the g-ratio is fairly constant across species and white matter regions (32,33) and is dependent mostly on the diameter of the axon according to the relationship presented in (34): $g_{ratio} = 0.220 * log(d_{unmyelinated}) + 0.508$ (see the plot on figure 2).

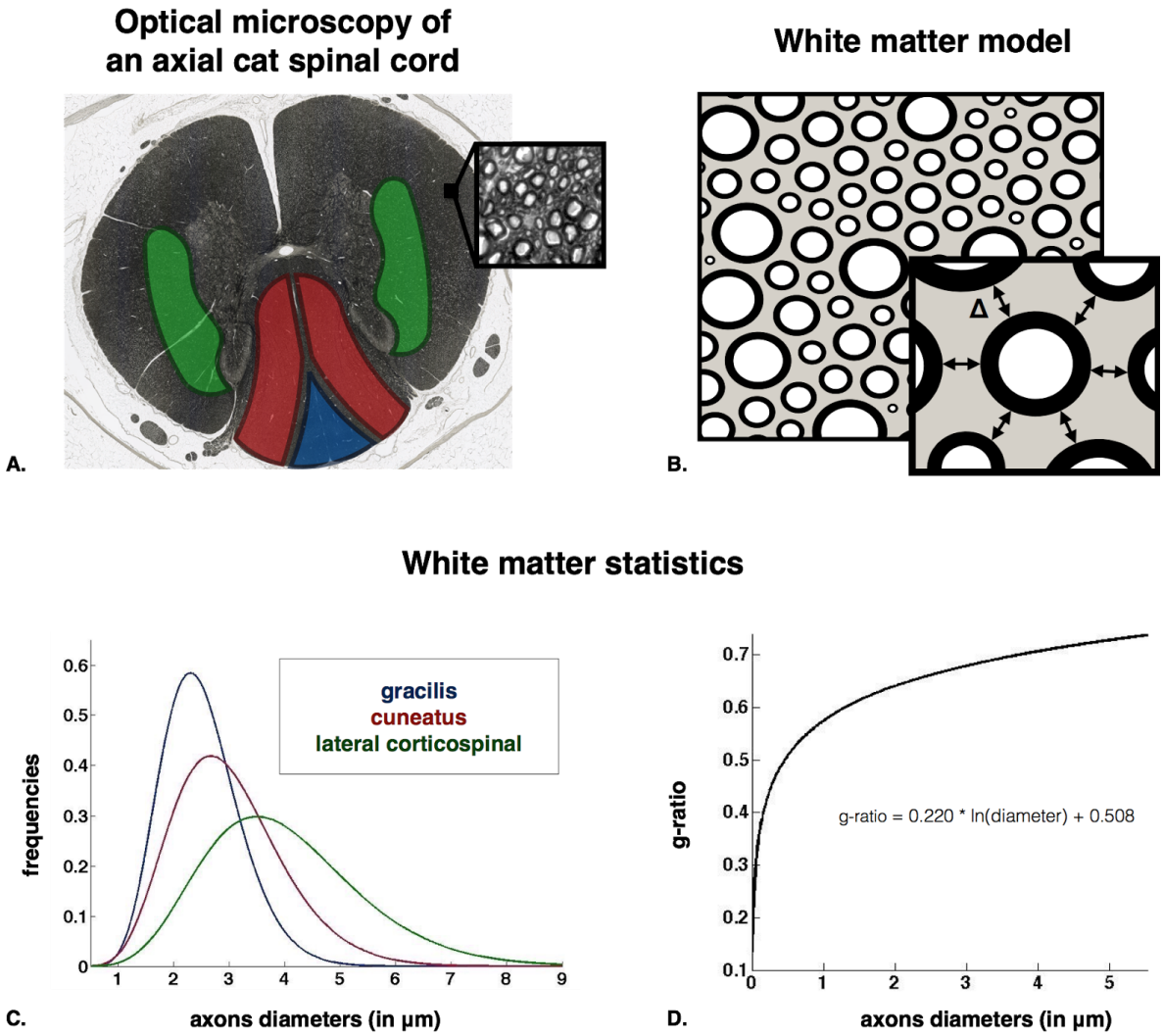

Figure 1 - AxonPacking model

A. Axial slice of cat spinal cord stained with osmium (color-coded for fiber diameter), adapted with permission from (5). Since most fibers are running along the spinal cord, axons appear like densely packed disks. Three regions can be identified: gracilis (blue), cuneatus (red) and lateral corticospinal (green). **B**. Corresponding Model of the white matter with three compartments: extra-axonal space (gray), myelin sheath (black), intra-axonal (white). Graphical illustration of the gap between axons Δ: the periphery of the center disk is at a distance Δ from the periphery of the other six disks in its neighborhood. **C**. Three Gamma probability density functions for three regions of the spinal cord: gracilis, cuneatus and lateral corticospinal (5). **D**. Relationship between the g-ratio and the axon diameters.

2.2. AxonPacking Algorithm

The simulator is implemented in Matlab (R2014a). The different steps to process packing are the following: (i) the diameters of the disks are randomly chosen using a Gamma distribution parameterized with the mean (μ), standard deviation (σ) and number of axons (N); (ii) the positions of disks are initialized on a grid, and then migrate toward the center of the packing area until the maximum disk density is achieved. A video illustrating the packing is available at: http://www.neuro.polymtl.ca/downloads.

The random disk diameters are obtained using a Hasting Metropolis algorithm (35). Briefly, from an initial diameter value, subsequent diameters are randomly drawn with a Gaussian law and accepted (or rejected) according to a probability depending on the Gamma probability density function. The acceptance probability over and under two fixed diameter values is forced to zero. These two thresholds (set to 0.2 and 10 μm by default) avoid unrealistically small or large axons. Figure 2.B shows an example of sampling for N = 1000 disks, μ = 3 μm and σ^2 = 1 μm. From the set of N disks following the expected diameter distribution, particle positions are initialized and then move along the iteration packing process according to specific rules. To take account for the gap Δ between the disks, the value Δ is added to each drawn diameter before performing the packing.

Initialization. The disks are randomly initialized on a grid within a square area. To initialize the disk positions in such a way that the disks do not overlap and are closed enough to each other the size of the square area is set to $\sqrt{N * (2 * max(R_k,\ k = 1..N) + \Delta)^2}$ (R_k the radii, Δ the gap between disks) and the spacing in height and width of the grid is set to the size of the square area divided by $\sqrt{N} + 1$. In this way every disk is initialized in a square of the grid whose side is larger than the disk diameter (figure 2.C).

Migrations. After that, at each iteration, every single particle migrates following the conditions defined in the next paragraph. At each iteration, the velocity of each disk is computed according to two different situations. In case of the absence of overlapping with any other disk, the velocity $\mathbf{V}_{att}$ is a constant attraction towards the center of the square area (figure 2.D). Its direction is computed from the positions of the disk and the center of the square area. Its norm is fixed to 0.01 μm/iteration. At each iteration, disk overlapping condition is checked by computing the matrix **P** of distance between pairs of disk. In case of

overlap (negative values in **P**), the velocity $\mathbf{V}_{rep}$ is the result of the repulsion between two disks. The direction of this velocity is defined by the center of the two disks that are in conflicts. If multiples disks are in conflict, the direction is calculated by summing all the individual velocities (figure 2.E). The norm of $\mathbf{V}_{rep}$ is fixed to a constant *c*. In order to discriminate the overlapping as much as possible, $||\mathbf{V}_{rep}||$ must be higher than $||\mathbf{V}_{att}||$ i.e $c > 0.01$ µm/iteration. However $||\mathbf{V}_{rep}||$ must be lower than the disk diameters to avoid bouncing of particles. It was found that a value of $c = 0.1$ µm/iteration is a good compromise between minimizing the total overlapping and attracting particle to a single point in order to reach high packing density without major bouncing of the disks. Note that *c* can be modified if necessary.

The disk density increases over the migrations and tends toward a limit value. It is necessary to first launch the algorithm with the packing inputs (N, µ, σ and Δ) and a high number of iterations: 35000 iterations when N = 1000 for example. MRI metrics such as the disks density e.g. FVF can be calculated every *p* iterations to assess the sufficient number of iterations to reach a certain degree of precision. *p* is a user-defined integer: $p = 250$ or 1000 for example. When the packing process is finished, the algorithm converts the packing image into a binary mask from which subsequent microstructure-related metrics can be derived: fiber volume fraction (FVF) e.g. the disk density, myelin volume fraction (MVF), axon volume fraction (AVF) and fraction of restricted water (*fr*). First a mask with three different labels (intra-axonal, myelin and extra-axonal) is generated in a control area A_{tot} that encompasses the center of the packing. The size of this area is chosen assuming a density of 1.6 after removing the empty spaces between disks. For each disk *i*, the intra-axonal and the myelin mask is computed using the associated g-ratio g_i. The microstructure parameters are computed using the following formulas:

$$FVF = \frac{A_{intra-axonal} + A_{myelin}}{A_{tot}} \qquad MVF = \frac{A_{myelin}}{A_{tot}} \qquad fr = \frac{A_{myelin}}{A_{myelin} + A_{extra-axonal}}$$

When every migration has been performed the overlapping area ratio $R_{overlap}$ between the disks is computed, which is the sum of the areas of overlap in the final packing divided by the total area of the disks (see figure 2.D): $R_{overlap} = A_{overlap} / A_{disks}$.

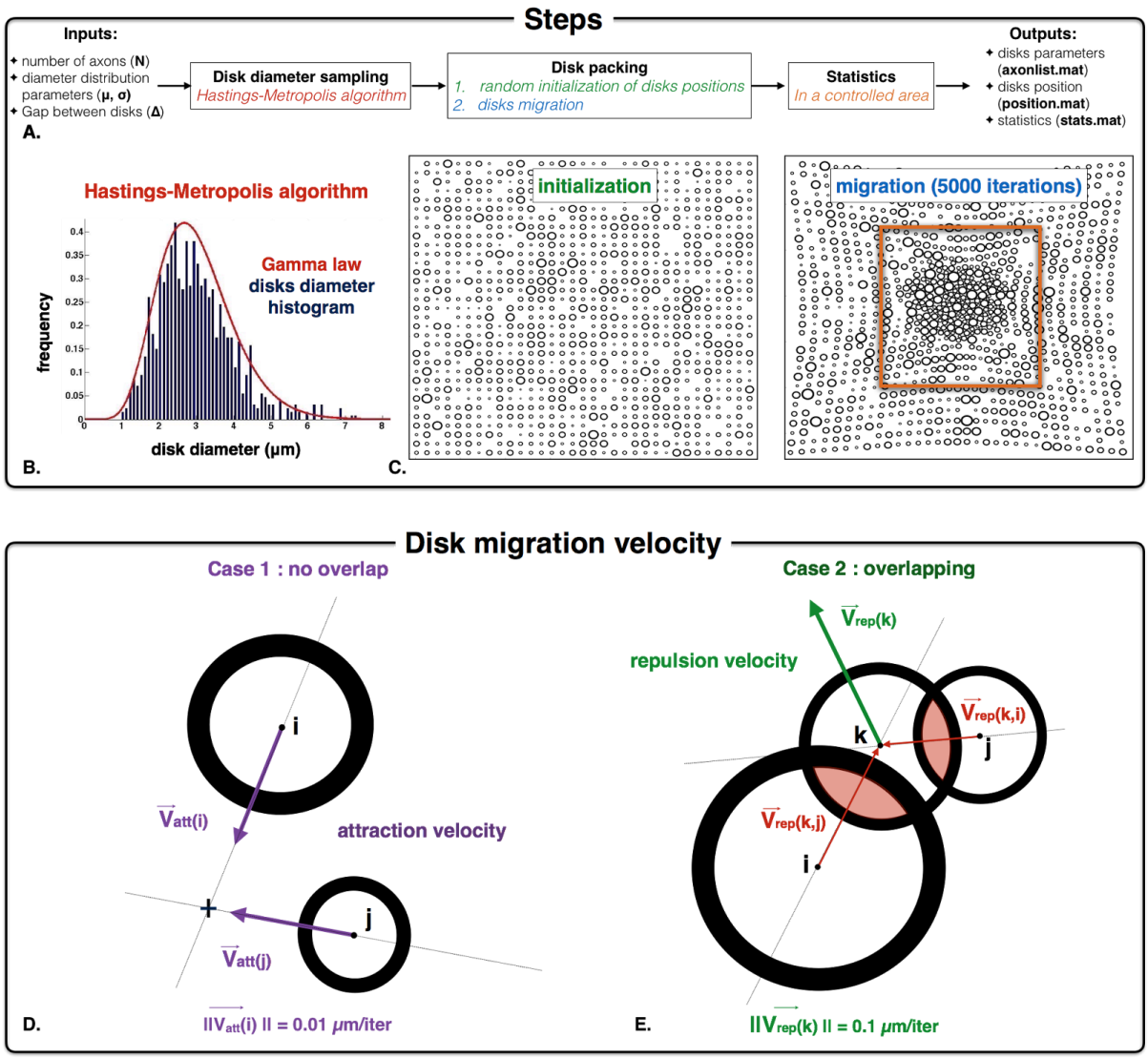

Figure 2 - AxonPacking algorithm

A. Overall procedure for disk packing algorithm. **B.** Histogram distribution of disk diameter. In this example, N = 1000 diameters are simulated, and the desire Gamma distribution of disks diameter is μ = 3 μm and σ^2 = 1 μm (red curve). Our implementation of the Hasting Metropolis algorithm generate disks diameter (blue histogram) that correctly match this distribution. **C.** Two steps in AxonPacking for the same example case (N=1000 disks). **D-E.** Graphical illustration of the attraction velocity that operates for every non-overlapping particles (**E**) and the repulsion velocity for the overlapping ones (**D**). The velocities are computed using the following equation: $V_{att}(i) = V_{att}(j) = 0.01$ μm/iteration. $V_{rep}(k) = c * (V_{rep}(k, i) + V_{rep}(k, j)) / || V_{rep}(k, i) + V_{rep}(k, j) ||$ with $V_{rep}(k, i) = (x_k - x_j , y_k - y_j)$ and c = 0.1 μm/iteration.

2.3. Validation in theoretical packing condition

Validation of the packing algorithm was performed using a well-known problem. The variance diameter σ^2 was set to 0 and a set of N = 250 disks with the same diameter (4 µm) were created. Based on mathematical theory, the highest disk density for one single diameter was obtained with a hexagonal structure (36). For such a Hexagonal Close Packing (HCP) the disk density is: $\phi_{HCP} = \pi / \sqrt{12} \simeq 0.907.$ The goal in this first section was to test whether the automatic packing converges towards a hexagonal structure.

2.4. Example application with known microstructure

AxonPacking was applied with known Gamma parameters (µ and σ) based on histology of the cervical spinal cord of cat (5): the mean diameter µ ranged from 2.5 to 3.5 µm and the standard deviation σ ranged from 0.5 to 2.5 µm.

2.4.1. Reproducibility over runs

Reproducibility over 50 runs was also studied for three different Gamma distributions of diameters that could be found in the spinal cord of cat: µ = 3 µm and σ^2 = [0.5, 1.5, 2.5] µm. The following parameters were used: N = 1000 disks, 30000 iterations and a gap Δ = 0. Then the standard deviation of FVF across runs was studied.

2.4.2. Stability of the final solution

In order to quantify the stability of the final density in the last iterations, the density FVF was computed every 250 iterations in a particular case (N = 1000 axons, µ = 3 µm, σ^2 = 1 µm, Δ = 0 and 35000 iterations is performed). The variation of FVF between 26000 and 35000 iterations was computed as follows:

$$\Delta(FVF) = max(FVF(26000 \leq iteration \leq 35000)) - min(FVF(26000 \leq iteration \leq 35000)).$$

2.4.3. Dependency of fiber volume fraction and myelin content on simulator parameters µ, σ and Δ.

The algorithm was applied with features specific to the white matter in the spinal cord of cat. Packings were made for three different Gamma distributions of inner diameters. Based on the existing axon segmentation (5) the diameter distributions is fitted with a Gamma law for different regions of the white matter and then three pairs (µ, σ^2) were chosen, representative

of three regions of the white matter: gracilis, cuneatus and lateral corticospinal. These regions are presented figure 1. For each set of axons six packings were performed with six different values for the gap: Δ = [0.1, 0.3, 0.5, 0.7, 0.9, 1.1] µm. The evolution of FVF, fr and MVF was assessed with respect to Δ for the three cases. N was set to 1000 and the number of iterations was set to 30000.

3. RESULTS

3.1. Hexagonal packing in monodisperse case

Figure 4 shows the packing at three stages of iterations: 0, 1000 and 7000. As expected from the theory, a hexagonal structure is obtained after convergence. The disk density calculated in the red rectangle for this packing after 7000 iterations is FVF = 0.892, which is close to the theoretical values FVF_{HCP} = 0.907 (2% error).The overlapping ratio is $R_{overlap} = 0.01\ \%$. Note that this simulation took 30 s on a iMac i5 3.4GHz (quad core).

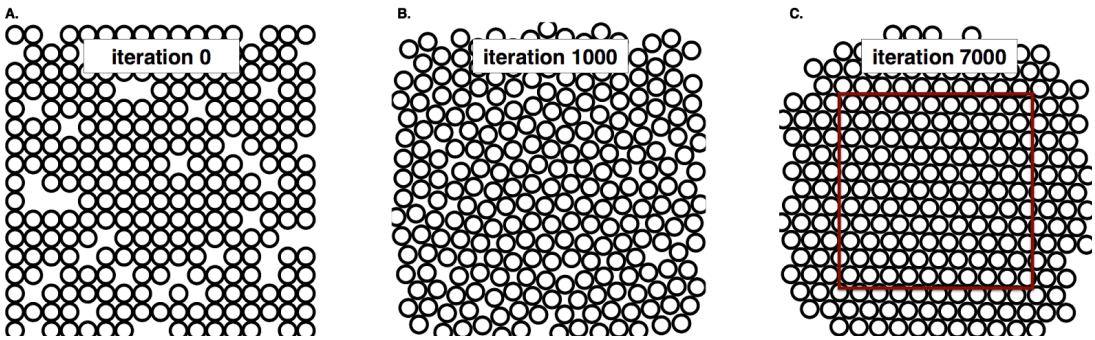

***Figure 4* - Iteration process for the Hexagonal packing in monodisperse case**

A. initial positions of the 250 disks. **B.** intermediate positions after 1000 migrations. **C.** final results after 7000 migrations.

3.2. Reproducibility over runs

Figure 5 shows the results of the simulation for the three different diameter distributions. The standard deviation for FVF over the 50 runs is lower than $3*10^{-3}$ in all 3 cases, demonstrating the good reproducibility over runs. In addition, these standard deviations are lower than the differences between the mean values ($>7*10^{-3}$), which shows that the simulator could distinguish significantly the different cases simulated. As a result, we found an optimal density, although very close, significantly bigger for the case with larger dispersion of axon

diameter (which corresponds to lateral corticospinal tract, see figure 1). Note that $R_{overlap}$ is lower than 0.1% for all packing simulations.

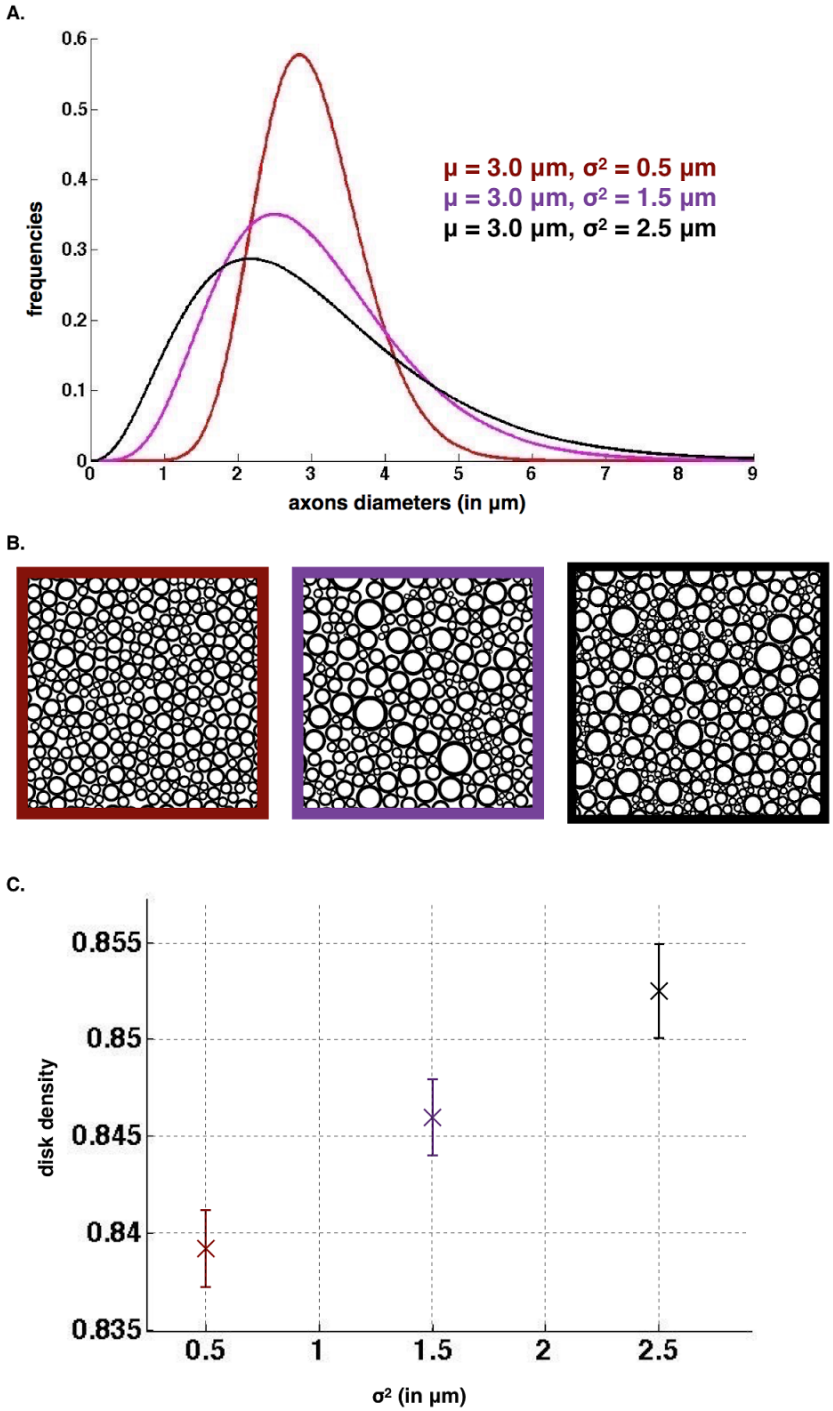

Figure 5 - Reproducibility of AxonPacking

A. Three diameters distributions. **B.** Final packing result for each distribution. **C.** Mean disk density with the standard deviation over the 50 runs for the three cases.

3.3. Stability of the final solution

Figure 6 shows the evolution of the disk density as a function of the iterations. The variation of the disk density over the last 9000 iterations is: Δ(FVF) = 0.8449 - 0.8440 < 0.001. For a fixed diameter distribution and N = 1000 particles the disk density FVF varies less than 0.001 after 26000 iterations. For these inputs (μ = 3 μm, σ^2 = 1 μm and Δ = 0) the algorithm can be stopped after 26000 iterations beyond which FVF don't vary anymore with a precision of 0.001.

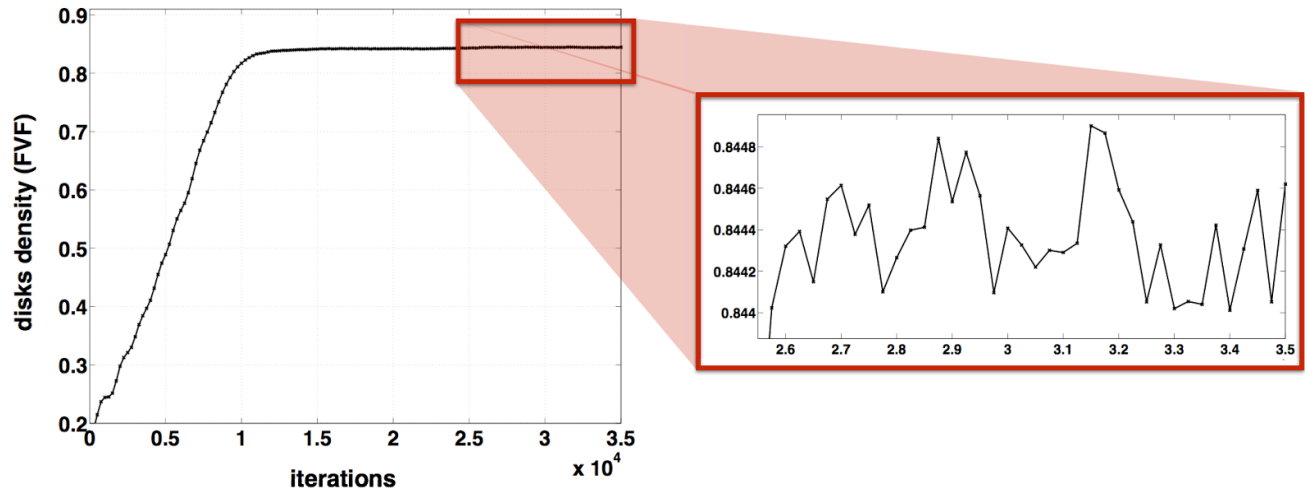

***Figure* 6 - Stability of AxonPacking**

Evolution of the disk density along the 35000 iterations for a packing of 1000 disks where μ = 3 μm, σ^2 = 1 μm and Δ = 0.

3.4. Application in the white matter

Figure 7 shows the resulting evolution of axonal density FVF, of the restricted volume fraction *fr* and the myelin volume fraction MVF when the distance between axons (Δ) varied from 0.1 to 1.1 μm, and for three regions of the spinal cord (cuneatus, gracilis and lateral corticospinal). Figure 1 shows the location of these regions and their respective typical diameter distributions. Figure 7A-C shows the range of values for FVF, *fr* and MVF for the three different regions. For each distribution, $R_{overlap}$ is lower than 0.005 % for Δ = 0.1 μm, null in every other cases. Note that each simulation took 40 min on a iMac i5 3.4GHz (quad core).

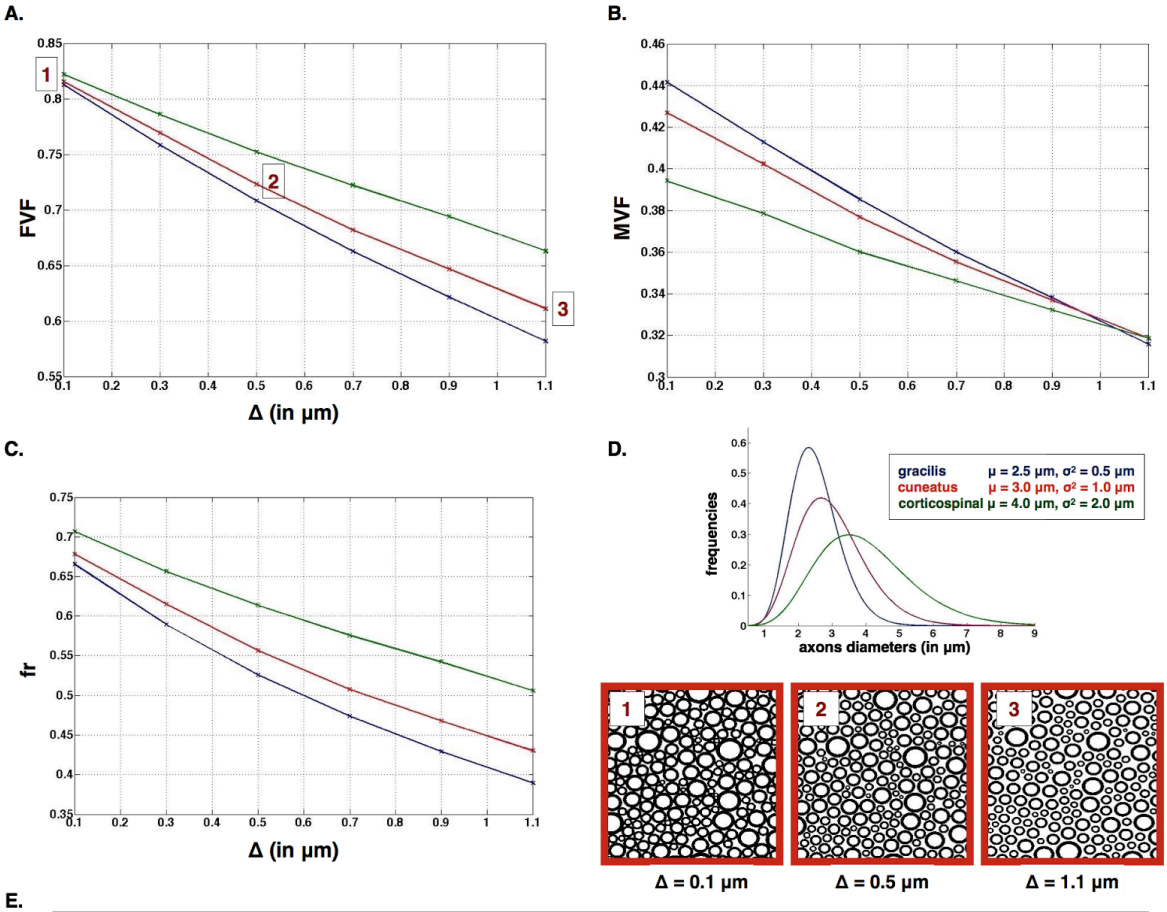

E.

Distribution parameters	Range for FVF	Range for *fr*	Range for MVF
µ = 2.5 µm, σ² = 0.5 µm	[0.81 - 0.58]	[0.67 - 0.39]	[0.44 - 0.32]
µ = 3.0 µm, σ² = 1.0 µm	[0.82 - 0.61]	[0.68 - 0.43]	[0.43 - 0.32]
µ = 4.0 µm, σ² = 2.0 µm	[0.82 - 0.66]	[0.71 - 0.51]	[0.39 - 0.32]

Figure 7 - Application for simulating white matter microstructure

A-C. Evolution of FVF, *fr* and MVF when different gaps between axons Δ are applied. **D. Top.** Three radii distribution function for the three spinal regions (blue: gracilis blue, red:cuneatus, green: lateral corticospinal) and associated Gamma parameters (µ,σ). **D. Bottom.** Packing results for cuneatus for three gaps Δ. **E.** Ranges of values for FVF, *fr* and MVF for the three regions: gracilis (first line), cuneatus (second line), lateral corticospinal (third line).

4. DISCUSSION

In this paper, a new algorithm for simulating dense packing of disks and particularly adapted to model the white matter is presented. The algorithm correctly converges toward an hexagonal packing in the monodisperse case and provides highly reproducible results. An application of the algorithm, presented in this manuscript, aimed to get the evolution for FVF, *fr* and MVF as a function of the gap between axons for different distributions found in the spinal cord of a cat. In this section, the performance and the limitations of AxonPacking will be discussed, results presented in figure 7 will be interpreted, and finally, the pros and cons of using AxonPacking to simulate the white matter will be detailed.

4.1. Validation and convergence of AxonPacking

AxonPacking was designed to optimize the density of the disks by migrating with a constant velocity the disks toward the center. As seen in the results section, the algorithm correctly converges toward the optimal solution in the configuration where all disks are identical: the final solution matches the hexagonal structure that is the theoretically highest reachable density for such a problem. However, in other configuration, such as in a bidisperse (two different diameters) or polydisperse disk packing configuration, no theoretical solution exists to calculate the highest density, and the solution provided by AxonPacking might not be optimal. Qualitatively however, we observe that only few empty space remain in the final solution. Also the final disk density is highly reproducible over runs (STD(FVF) < 0.003), no matter the initialization of the disks on the initial grid, suggesting that the final solution is physically optimal for particle dynamics.

It should be noted that this variation over runs is lower than the variation for FVF over different regions of white matter obtained with histology. In corpus callosum FVF ranges between 0.47 and 0.76 over genu, body and splenium regions (37). As a consequence the packing algorithm can be considered precise enough to differentiate regions defined by specific combination of (μ, σ, Δ). The stability and the reproducibility was observed for axon diameters distribution which come from the histology of the cat spinal cord. In the future AxonPacking could be applied to other species exhibiting different microstructure properties, such as monkey (38), human (39) or rat (40).

In this algorithm some overlapping is tolerated. However the residual overlapping area is negligible (<0.1 for all the packings presented in this paper). This good performance is obtained by turning off the constant velocity toward the center when overlapping occurs.

Figure 6 shows that the optimal solution, although very stable, oscillates toward an optimal value. This oscillation is attributed to the rebounce between disks, that was minimized by using velocities much smaller than the particles diameter (0.01 µm/iteration for attraction and 0.1 µm/iteration for repulsion versus diameters >0.2 µm). No stopping criteria was implemented here. Instead, the number of iterations was set to a large value (N=30000), that was experimentally found to be sufficient to obtain a stable solution in our simulations (see one example in figure 6). Results part 4.3 showed that the standard deviation of FVF over 50 runs for three different diameter distributions and 26000 iterations is lower than 0.001.

Thanks to the good reproducibility of the simulations, we were able to generate a dataset of axon packing for a variety of diameter distributions, gaps Δ and fiber density[3]. Also, results from section 4.4 can be used as a lookup table to estimate parameters *fr*, MVF or FVF knowing the diameter distribution and one of the three parameters without running the simulator.

4.2. Using AxonPacking for modeling white matter

AxonPacking makes a couple of assumption and simplifications in order to model the white matter. First, the algorithm assumes perfectly circular and non-deformable axons. This choice was motivated by the observation that most of the axons are qualitatively circular on electron microscopy or coherent anti-stokes Raman spectroscopy (5,41,42). However, axons, and more particularly the large ones, can show some deformation with more elliptical or even tortuous shapes. These deformations would allow slightly higher density that the ones found in this work. Future work could consider controlled deformations of the particle shape.

Second, AxonPacking assumes a fixed gap Δ between axons. This gap is necessary to leave enough space for the extracellular matrix and the glial cells. As observed in histological images, there exists a variation of the average gap between axons (5) that could be attributed to different category and proportion of glial cells between regions (43). In this work, the goal was to find the global effect of this variation of gap between axons on metrics *fr*, MVF and FVF. However, a fixed gap in each regions is a strong assumption that could be refined by considering a distribution of gap.

[3] https://github.com/neuropoly/axonpacking/tree/master/results

Third, AxonPacking assumes that axons are packed with maximum density, as suggested by the natural tendency of white matter organization (44). While this trends might deviate from the true organization across white matter pathways and peripheral nerves, across species and pathologies, this assumption can be acceptable in some instances, as corroborated by the example application in the cat spinal cord (Figure 7). Moreover, the gap between axons can always be adjusted by the user if necessary.

Fourth, AxonPacking considers that axon fibers are parallel. While this assumption doesn't hold in regions that present a fanning or tortuosity of the fibers, this assumption holds in a couple of structures of the central nervous system such as the spinal cord. This is confirmed in the spinal cord by a consistency of microstructural MRI metrics (axon diameter index, fiber density) along the spinal cord (45).

Fifth, white matter is not only composed of myelinated axons but also contains blood vessels, nerve cells body, fissures and lakes containing cerebrospinal fluid. In future work, more realistic representation of the white matter can be included in the packing algorithm.

Finally, all axons in AxonPacking are myelinated axons. While non-myelinated axons also exist in the white matter (38,46), their fraction is generally small. For example, the myelinated-to-unmyelinated ratio ranges from 0.69 to 0.97 in the monkey corpus callosum (38). Moreover, the mean diameter of the unmyelinated fibers is much smaller than the myelinated one, respectively 0.18 µm and 2.2 µm (46), which somewhat minimizes the impact of unmyelinated fibers on the calculation of FVF. Again, future work can address this issue if desired by the modeling study.

4.3. Simulating the variation of *fr*, MVF and FVF in the white matter

Result section "Application in the white matter" shows how FVF, *fr* and MVF vary as a function of Δ (distance between axons) for different diameter distributions. Several observations can be reported.

First, for a gap Δ=0, a change in diameter distribution mostly impacts MVF (10% variation in our simulations) and *fr* (~7% variation) with inverse trends. The presence of large axons lowers MVF because large axons have bigger g-ratio and thus proportionally less myelin (see figure 1.D). Thinner myelin leaves space for the intra-axonal water, increasing *fr*. We observe, however, very small impact on FVF (~1%).

Second, the difference of FVF between the three configurations of axon diameter increases while the inter-axon gap Δ increases. Indeed, for regions presenting large axons, a small

gap (e.g. $\Delta < 0.1*\mu$) only has a small impact on the calculated volume fractions. However, in axon diameters are small, a smaller gap will yield a drop of FVF. A reduction of FVF consequently leads to a proportional reduction of *fr* and MVF, which then leads to a convergence of MVF between the three configurations, and a divergence of *fr*, when increasing the gap Δ. Hence, while *fr* is highly sensitive to the mean axon diameter for any gaps Δ, MVF is robust to the mean axon diameter when the ratio Δ/μ is close to 0.3. In this regime, MVF is driven mostly by the gap between axons and by the g-ratio.
Note that the curves reported on figure 7 can also be used to choose the right gap Δ in order to generate synthetic axonal packing with particular fiber density or myelin volume fraction.

5. CONCLUSION

AxonPacking is a novel open-source algorithm for simulating white matter microstructure, in which axons are assumed to be parallel cylinders. AxonPacking generates random disk packing with user-defined diameter distribution and gap between the disks and then compute the following microstructure features: MVF, FVF and *fr*. AxonPacking has been applied with three different diameter distributions specific to the white matter in the spinal cord and a range of gaps to get the dependency of MVF, FVF and *fr* regarding the different configuration of axon size and packing density. AxonPacking can be useful for the study of qMRI methods applied to the peripheral and central nervous system.

6. ACKNOWLEDGMENTS

We thank the MS Society of Canada (Duval, #2370), the SensoriMotor Rehabilitation Research Team (SMRRT) of the Canadian Institute of Health Research, the Canada Research Chair in Quantitative Magnetic Resonance Imaging (JCA), the Canadian Institute of Health Research [CIHR FDN-143263], the Fonds de Recherche du Québec - Santé [28826], the Fonds de Recherche du Québec - Nature et Technologies [2015-PR-182754], the Natural Sciences and Engineering Research Council of Canada [435897-2013] and the Quebec BioImaging Network. We also thank people of the NeuroPoly laboratory and in particular Victor Herman and Aldo Zaimi.

7. REFERENCES

1. Laule C, Vavasour IM, Kolind SH, Li DKB, Traboulsee TL, Moore GRW, MacKay AL. Magnetic resonance imaging of myelin. Neurotherapeutics 2007;4:460–484.

2. Assaf Y, Blumenfeld-Katzir T, Yovel Y, Basser PJ. AxCaliber: a method for measuring axon diameter distribution from diffusion MRI. Magn. Reson. Med. 2008;59:1347–1354.

3. Stikov N, Perry LM, Mezer A, Rykhlevskaia E, Wandell BA, Pauly JM, Dougherty RF. Bound pool fractions complement diffusion measures to describe white matter micro and macrostructure. Neuroimage 2011;54:1112–1121.

4. Zhang H, Schneider T, Wheeler-Kingshott CA, Alexander DC. NODDI: practical in vivo neurite orientation dispersion and density imaging of the human brain. Neuroimage 2012;61:1000–1016.

5. Zaimi A, Duval T, Gasecka A, Côté D, Stikov N, Cohen-Adad J. AxonSeg: Open Source Software for Axon and Myelin Segmentation and Morphometric Analysis. Front. Neuroinform. 2016;10:37.

6. Isola R. Packing of granular materials. University of Nottingham; 2008.

7. Zhang HP, Makse HA. Jamming transition in emulsions and granular materials. Phys. Rev. E Stat. Nonlin. Soft Matter Phys. 2005;72:011301.

8. Yu AB, Bridgwater J, Burbidge A. On the modelling of the packing of fine particles. Powder Technolology 1997;92:185–194.

9. Williams SR, Philipse AP. Random packings of spheres and spherocylinders simulated by mechanical contraction. Phys. Rev. E Stat. Nonlin. Soft Matter Phys. 2003;67:051301.

10. Bernal JD, Mason J. Packing of Spheres: Co-ordination of Randomly Packed Spheres. Nature 1960;188:910–911.

11. Dowsland KA. Optimising the palletisation of cylinders in cases. OR Spektrum 1991;13:204–212.

12. Sugihara K, Sawai M, Sano H, Kim D-S, Kim D. Disk packing for the estimation of the size of a wire bundle. Jpn. J. Ind. Appl. Math. 2004;21:259–278.

13. Collins CR, Stephenson K. A circle packing algorithm. Comput. Geom. 2003;25:233–256.

14. Lenstra JK, Rinnooy AH. Complexity of packing, covering and partitioning problems. Econometric Institute; 1979.

15. Mackay AL. A dense non-crystallographic packing of equal spheres. Acta Crystallogr. 1962;15:916–918.

16. Gensane T. Dense packings of equal spheres in a cube. The Electronic Journal of Combinatorics 2004;11:1–17.

17. Stoyan Y, Yaskov G. Packing Identical Spheres into a Rectangular Parallelepiped. In: Bortfeldt A, Homberger J, Kopfer H, Pankratz G, Strangmeier R, editors. Intelligent Decision Support. Gabler; 2008. pp. 47–67.

18. Locatelli M, Raber U. Packing equal circles in a square: a deterministic global optimization approach. Discrete Appl. Math. 2002;122:139–166.

19. Graham RL, Lubachevsky BD, Nurmela KJ, Östergård PRJ. Dense packings of congruent circles in a circle. Discrete Math. 1998;181:139–154.

20. George JA, George JM, Lamar BW. Packing different-sized circles into a rectangular container. Eur. J. Oper. Res. 1995;84:693–712.

21. Stoyan YG, Yas'kov G. A mathematical model and a solution method for the problem of placing various-sized circles into a strip. Eur. J. Oper. Res. 2004;156:590–600.

22. Wang H, Huang W, Zhang Q, Xu D. An improved algorithm for the packing of unequal circles within a larger containing circle. Eur. J. Oper. Res. 2002;141:440–453.

23. Belevičius R, Kačianauskas R, Markauskas D, Šešok D. Packing of Polydispersed Discs into Containers of Regular Shape. Part. Sci. Technol. 2011;29:28–39.

24. Bagi K. An algorithm to generate random dense arrangements for discrete element simulations of granular assemblies. Granular Matter 2005;7:31–43.

25. Donev A, Torquato S, Stillinger FH. Neighbor list collision-driven molecular dynamics simulation for nonspherical hard particles. I. Algorithmic details. J. Comput. Phys. 2005;202:737–764.

26. Frenkel D, Smit B. Understanding Molecular Simulation. From algorithms to applications. 2nd ed. Academic Press; 2006.

27. Lubachevsky BD. How to simulate billiards and similar systems. J. Comput. Phys. 1991;94:255–283.

28. Hall MG, Alexander DC. Convergence and parameter choice for Monte-Carlo simulations of diffusion MRI. IEEE Trans. Med. Imaging 2009;28:1354–1364.

29. HY. Mesri, DS Novikov, MA Viergever, A Leemans. Simulating axon packing for investigating white matter tissue characteristics with diffusion MRI. In: Proceedings of the 24th Annual Meeting of ISMRM. ; 2016. p. 3084.

30. Pajevic S, Basser PJ. An optimum principle predicts the distribution of axon diameters in normal white matter. PLoS One 2013;8:e54095.

31. Sepehrband F, Alexander DC, Clark KA, Kurniawan ND, Yang Z, Reutens DC. Parametric Probability Distribution Functions for Axon Diameters of Corpus Callosum. Front. Neuroanat. 2016;10:59.

32. Chomiak T, Hu B. What is the optimal value of the g-ratio for myelinated fibers in the rat CNS? A theoretical approach. PLoS One 2009;4:e7754.

33. Rushton WAH. A theory of the effects of fibre size in medullated nerve. J. Physiol. 1951;115:101–122.

34. Ikeda M, Oka Y. The relationship between nerve conduction velocity and fiber morphology during peripheral nerve regeneration. Brain Behav. 2012;2:382–390.

35. Chib S, Greenberg E. Understanding the Metropolis-Hastings Algorithm. Am. Stat. 1995;49:327–335.

36. Chang H-C, Wang L-C. A Simple Proof of Thue's Theorem on Circle Packing. arXiv [math.MG] [Internet] 2010.

37. Stikov N, Campbell JSW, Stroh T, et al. Quantitative analysis of the myelin g-ratio from electron microscopy images of the macaque corpus callosum. Data Brief 2015;4:368–373.

38. Lamantia AS, Rakic P. Cytological and quantitative characteristics of four cerebral commissures in the rhesus monkey. J. Comp. Neurol. 1990;291:520–537.

39. Aboitiz F, Scheibel AB, Fisher RS, Zaidel E. Fiber composition of the human corpus callosum. Brain Res. 1992;598:143–153.

40. Leenen LP, Meek J, Posthuma PR, Nieuwenhuys R. A detailed morphometrical analysis of the pyramidal tract of the rat. Brain Res. 1985;359:65–80.

41. Perge JA, Niven JE, Mugnaini E, Balasubramanian V, Sterling P. Why do axons differ in caliber? J. Neurosci. 2012;32:626–638.

42. Bégin S, Dupont-Therrien O, Bélanger E, Daradich A, Laffray S, De Koninck Y, Côté DC. Automated method for the segmentation and morphometry of nerve fibers in large-scale CARS images of spinal cord tissue. Biomed. Opt. Express 2014;5:4145–4161.

43. Olude MA, Mustapha OA, Aderounmu OA, Olopade JO, Ihunwo AO. Astrocyte morphology, heterogeneity, and density in the developing African giant rat (Cricetomys gambianus). Front. Neuroanat. 2015;9:67.

44. Perge JA, Koch K, Miller R, Sterling P, Balasubramanian V. How the optic nerve allocates space, energy capacity, and information. J. Neurosci. 2009;29:7917–7928.

45. Duval T, McNab JA, Setsompop K, Witzel T, Schneider T, Huang SY, Keil B, Klawiter EC, Wald LL, Cohen-Adad J. In vivo mapping of human spinal cord microstructure at 300mT/m. Neuroimage 2015;118:494–507.

46. Biedenbach MA, De Vito JL, Brown AC. Pyramidal tract of the cat: axon size and morphology. Exp. Brain Res. 1986;61:303–310.